

## SIMULATION STUDY ON LIGHT VECTOR MESON DECAYS TO ELECTRON–POSITRON PAIRS WITH THE ALICE EXPERIMENT

*B. Batyunya, M. Vala, S. Zaporozhets  
for ALICE Collaboration*

Joint Institute for Nuclear Research, Dubna

Simulation study on  $\omega$ ,  $\phi$ ,  $\rho$  decays to  $e^+e^-$  pairs in the ALICE detector for Pb–Pb collisions at LHC energy was performed. The possibility of selecting resonance signals over the combinatorial backgrounds is demonstrated using the realistic simulation tracking and particle identification algorithms of the ALICE offline framework (AliRoot). Results for  $J/\psi$  are presented also for comparison.

Выполнено исследование моделирования распадов  $\omega$ -,  $\phi$ - и  $\rho$ -мезонов на электрон-позитронные пары в центральном детекторе эксперимента ALICE при взаимодействии ядер свинца с энергией ЛHC. Показана возможность выделения этих резонансов над комбинаторным фоном с помощью программ реалистичного моделирования детектора, восстановления треков и идентификации частиц, входящих в состав набора программ обработки эксперимента AliRoot. Для сравнения приводятся результаты выделения  $J/\psi$ -резонанса.

PACS: 25.75.Dw, 29.85.Fj, 29.20.db

### INTRODUCTION

The production of light vector mesons is expected to provide detailed information on the reaction dynamics of ultra-relativistic nucleus–nucleus collisions. Changes in resonances line-shape are expected in heavy-ion collisions for two reasons: (i) a dense medium can induce significant collision broadening [1–4]; (ii) shifts of both mass and width could be produced as a result of partial chiral symmetry restoration which is expected to occur together with deconfinement [5,6]. As a consequence, the width broadening is predicted up to 450, 100 and 80 MeV for  $\rho$ ,  $\omega$  and  $\phi$  mesons, respectively [4]. Thus, these predicted widths are  $\sim 3$ ,  $\sim 12$  and  $\sim 20$  times larger than the corresponding experimental ones presented in the Particle Data Group (PDG). The prediction of very strong mass decrease for  $\rho$  and of mass decrease up to 150 MeV for  $\phi$  has been done also [6].

To study the early stage of the heavy-ion collisions the resonance decays to dileptons are more preferable than to hadrons because leptons do not interact strongly and carry information on the early state would be more appropriate. A significant excess of dilepton pairs (with pair masses below  $1 \text{ GeV}/c^2$ ) above the yield expected from neutral mesons decay, has been observed firstly by the NA45(CERES) experiment at the CERN SPS for 200A GeV S–Au collisions [7]. The same effect has been shown also for different heavy-ion interactions and at different energies [8–13].

The  $\phi$  meson is of particular interest owing to its ( $s\bar{s}$ ) valence quark content, which makes  $\phi$  a signature of strangeness production mechanism from a possible early partonic phase [14, 15]. An enhancement of  $\phi$  production by a factor of 3–10 with respect to  $p$ – $p$  interactions (at the same energy) was proposed [16] as a quark–gluon plasma (QGP) signature, or alternatively as a result of the secondary collisions of partons and hadrons in the dense nuclear matter. The  $\phi$  decay will be observed in ALICE (A Large Ion Collider Experiment) [17–19] both in leptonic and hadronic channels and the ratio of the decay widths in these two decay channels might be very sensitive to changes in strange quark or kaon masses [1, 2]. Recent SPS Pb–Pb [20] and RHIC Au–Au [21–23] results show that no change of the mass or width is observed at SPS and RHIC energies. But, at the same time, a rise of the slope parameter by a factor of 1.7 in the transverse momentum spectra and an enhancement of the  $\phi/\pi$  ratio by a factor of 3 as compared to the minimum-bias  $p$ – $p$  interactions were found [20, 24]. Comparison of  $\phi$  decays to kaons and leptons did not give completely clear answers, since the differences of the distributions on  $p_t$  and rapidity observed firstly for  $\phi \rightarrow K^+K^-$  in the NA49 experiment [20] and for  $\phi \rightarrow \mu^+\mu^-$  in NA50 one [25] at SPS energy have not been confirmed by the results of the NA45 [26] and NA60 [27] experiments.

The simulation results of the expected experimental mass spectrum of ( $K^+K^-$ ) pairs and  $\phi \rightarrow K^+K^-$  decay detection in ALICE were reported in [28] (see also Subsec. 11.4.3 in [17] and Subsec. 6.2.5 in [19]). Also preliminary results for  $\rho^0 \rightarrow \pi^+\pi^-$  signal reconstruction can be found in [19] (in Subsec. 6.2.4). Here we present the first simulation results for detection capability of light vector meson decays to dielectron ( $e^+e^-$ ) pairs in ALICE for Pb–Pb collisions. The AliRoot framework (see Ch. 4 in [18]) was used for detectors simulation, tracking and particle identification (PID). Details on the detector efficiencies, track reconstruction algorithms and PID efficiencies can be found in Ch. 5 of [19]. The following outline will be adopted: firstly the simulation method will be introduced in Sec. 1 for detailed and fast steps of the simulation, then the results for effective mass spectra will be presented and discussed in Sec. 2, finally the results will be summarized in Conclusions.

## 1. SIMULATION METHOD

The main experimental and simulation problem in selecting of  $\rho^0$ ,  $\omega$  and  $\phi$  decays to dileptons is very small branching ratios of these modes. In addition, a very high combinatorial background is expected in heavy-ion collisions at the LHC energy from the different sources:  $\pi^0$ ,  $\eta$ , charmed and beauty particle decays, gamma conversions and misidentified electrons and positrons. It is clear that, in such conditions, very good  $e^\pm$  identification and the best possible signal-to-background ratio (S/B) are required.

The general simulation method consisted of two steps:

- detailed simulations of the detectors using the GEANT3 package inside the AliRoot framework, tracking and  $e^\pm$  PID to find the necessary tracking and PID efficiencies and momentum ( $p$ ) and angular resolutions for the reconstructed tracks;
- fast simulation of ( $e^+e^-$ ) pairs detection and analysis using very fast generators and the efficiencies and track resolutions obtained at the first step.

**1.1. The First (Detailed) Step of the Simulation.** A detailed simulation of the Inner Tracking System (ITS, [29]), the Time Projection Chamber (TPC, [30]) and the Transition

Radiation Detector (TRD, [31, 32]) was used for the tracking and  $e^\pm$  identification. The magnetic field of 0.5 T was taken for the simulation.

Figure 1, *a* shows the dependences of physical track-finding efficiency for electrons on transverse momentum ( $p_t$ ) in acceptance of the detectors under study: in the full azimuthal angle ( $\varphi$ ) range and in the pseudo-rapidity region,  $-0.9 \leq \eta \leq 0.9$ . We mean by the «physical track-finding efficiency» the ratio of the number of reconstructed electron tracks to the generated ones. The dependences of these efficiencies for electrons on polar ( $\theta$ ) and azimuthal ( $\varphi$ ) angles are shown in Fig. 1, *b, c*. To obtain these results the «Box» generator in the AliRoot with uniform  $p_t$  and  $\eta$  distributions was used. Ten events with 4000 electrons per event have been processed. One can see from Fig. 1 that the tracking efficiency is higher than 0.7 in almost all  $p_t$  regions and does not depend on  $\theta$  angle in the detector acceptance, ( $-45 \leq \theta \leq 135^\circ$ ) and has the strong decreases in the  $\varphi$  dependence corresponding to the dead regions between the next modules in the TPC and TRD.

To get momentum and angular resolutions for electron tracks reconstructed in the ITS and TPC, the events containing 4000 of  $\phi \rightarrow e^+e^-$  decays were processed using the AliGenParam generator of the AliRoot. It can generate an arbitrary number of different type of particles (with Poisson distribution) having the uniform pseudo-rapidity distribution in the acceptance under study and exponential  $p_t$  distribution obtained from the  $M_t$  scaling functions. The decays of the particles are performed using the PYTHIA generator [33]. Figure 2, *a* shows the dependence of the relative  $p_t$  resolution ( $\delta p_t/p_t$  in %) on  $p_t$  at  $p_t \geq 1$  GeV/c for  $e^\pm$ , i.e., in the range of effective  $e^\pm$  selection in the TRD. The  $\delta p_t$  has been obtained as the difference between generated and reconstructed transverse momenta of  $e^\pm$ . The asymmetric tail is caused by the bremsstrahlung effect which has not been taken into account in the track reconstruction algorithms. It should be noted that Gaussian sigma is near 0.7% in the Gaussian part of the distribution. It was found also that average angular resolution is near 1 mrad for both  $\theta$  and  $\varphi$  angles in the  $p_t$  range of  $e^\pm$  under study.

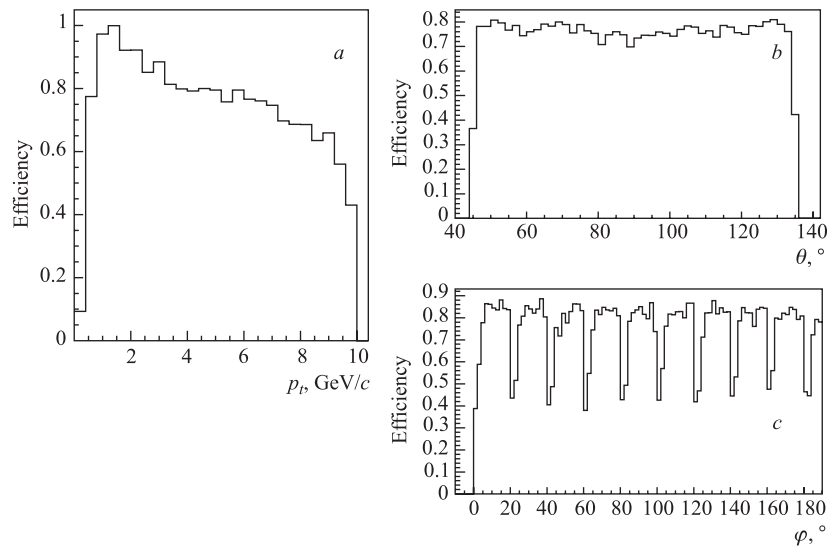


Fig. 1. Dependences of tracking efficiency for electrons on  $p_t$  (*a*), on polar angle ( $\theta$ ) (*b*) and on azimuthal angle ( $\varphi$ ) (*c*) for the tracks reconstructed in the ITS, TPC and TRD

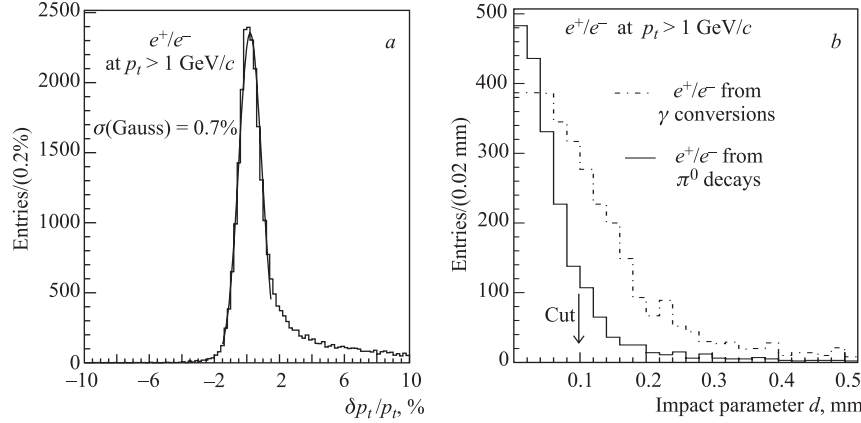


Fig. 2. a) Transverse momentum relative resolution  $\delta p_t$  for  $e^\pm$  tracks reconstructed in the ITS and TPC. b) Distributions on impact parameter in transverse plane (see text) for  $e^\pm$  from gamma conversions and from  $\pi^0$  decays

To study possible rejection of  $e^\pm$  contribution from gamma conversions 5700 events generated by HIJINGparam generator in the AliRoot were processed through the simulation and reconstruction packages of the ITS, TPC and TRD. An event of the generator included 12 000 neutral and charged pions and kaons (in the acceptance under study) with their decays and with realistic  $K/\pi$  ratio (near 0.13). The rapidity and  $p_t$  distributions of primary particles are the same as in the AliGenParam generator. The distributions on transverse impact parameter ( $d$ ), the nearest distance from track to primary vertex in the transverse plane, were analyzed. Figure 2, b shows these distributions for  $e^\pm$  from gamma conversions and from  $\pi^0$  decays. Only tracks with reconstructed points in all six layers of the ITS and at  $p_t \geq 1$  GeV/c have been taken. One can see from Fig. 2, b that distribution is significantly wider for  $e^\pm$  from gamma conversions. It was found that 43% of  $e^\pm$  from gamma conversions can be removed at 18% loss of  $e^\pm$  from  $\pi^0$  decays using the cut  $d \leq 0.1$  mm.

The  $e^\pm$  identification was done using the TPC and TRD combination for the PID. The most important question was for a possible pion rejection factor depending on the particle momentum for events with very high charged particle multiplicity. The values of this factor of (25–500) were obtained in the TRD for single particle in the beam-test and simulation at different particle momenta by the different PID methods and at  $e^\pm$  efficiency 90% (Subsec. 5.4.3 in [19], Subsec. 3.3 in [34]). It was shown also by the simulation that the pion rejection in the TRD decreases by factor of 1.5 and 2 at charged particle density 3000 and 6000, respectively, for pion momentum of 2 GeV/c (Sec. 11.5 in [32]).

To study this problem special events were generated using the AliGenCocktail generator (inside the AliRoot) which can create any combinations of the AliGenParam one. These events included 12 000  $\pi^\pm$  (mean number from Poisson distribution) in the full momentum region and, in addition, 20 particles of each species ( $e^\pm$ ,  $\pi^\pm$ ,  $K^\pm$  and  $p/\bar{p}$ ) at  $p_t \geq 1$  GeV/c (in the PID region of the TRD). As a result, the charged particle density,  $dN_{ch}/dy$ , of the events was equal to  $\sim 5000$ .

To calculate the  $\pi^\pm$  rejection factors at the fixed  $e^\pm$  efficiencies in the TRD, the  $L_{QX}$  likelihood method was used (see, for example, Subsec. 14.3.5 in [32] and Subsec. 5.4.3 in [19]).

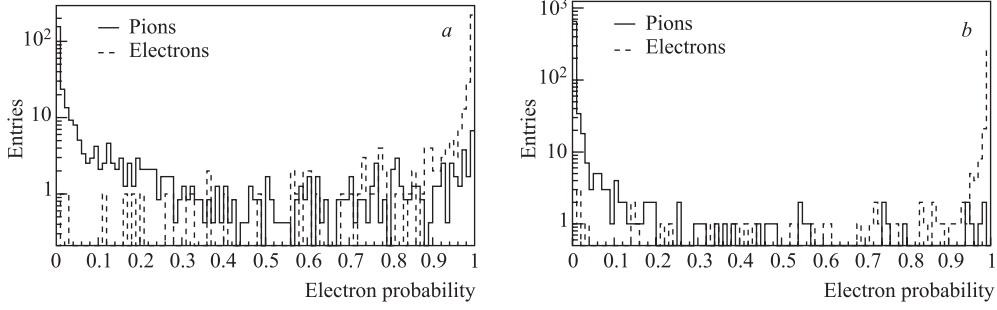


Fig. 3. Likelihood probabilities for electrons ( $e^\pm$ ) and pions at momentum 6 GeV/c identified as electrons in the TRD (a) and in the TRD and TPC combination (b)

The probabilities for  $e^\pm$ ,  $\pi^\pm$ ,  $K^\pm$  and  $p/\bar{p}$  at fixed momentum and certain energy deposit for each TRD layer were taken from the special class of the TRD simulation package in the AliRoot. Figure 3, a shows, for example, distributions of the likelihood  $e^\pm$  probabilities (electron probability in the figure) calculated for  $e^\pm$  and  $\pi^\pm$  detected in the TRD at momentum 6 GeV/c.

The probabilities for the TPC were calculated using the energy loss ( $dE/dx$ ) information stored in the AliRoot output root file. Figure 4 shows the TPC signals obtained by the truncated mean method (see Subsec. 7.4.4 in [30]) for  $e^\pm$ ,  $\pi^\pm$ ,  $K^\pm$  and  $p/\bar{p}$  in the momentum interval  $\delta p = 0.1$  GeV/c around momenta 2, 4, 6, 8 GeV/c.

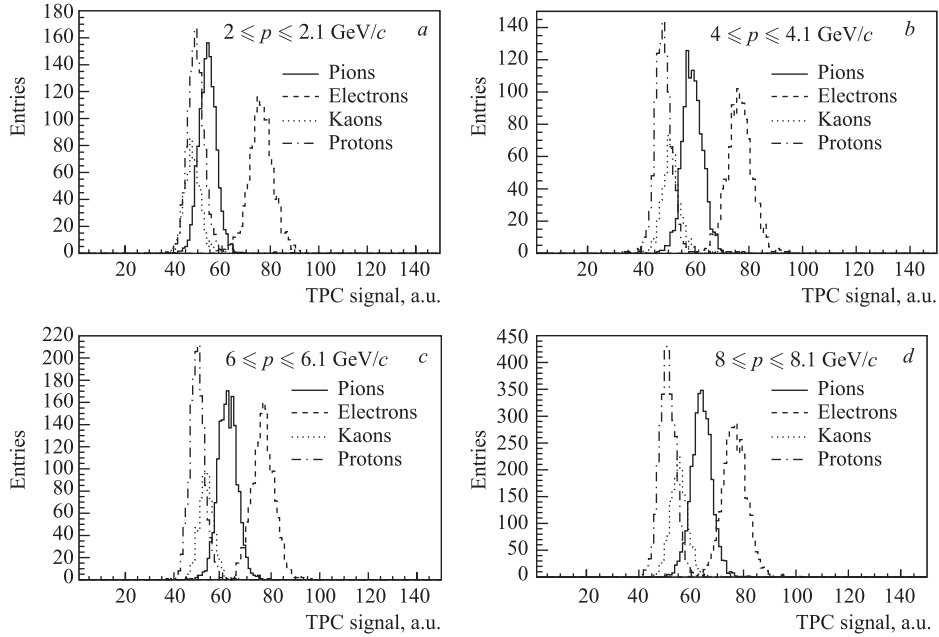


Fig. 4. Distributions on the TPC signals (in arbitrary units) obtained by the truncated mean method (Subsec. 7.4.4 in [30]) for different particles at different momenta

One can see from Fig.4 that selection possibility of  $e^\pm$  is good enough in all shown momentum region and becomes worse as the momentum increases.

The result for the likelihood probability but for combination of the TRD and TPC is presented in Fig.3,*b*. It is seen that the separation possibility between  $e^\pm$  and  $\pi^\pm$  is much better for the combination of these two detectors as compared with the TRD only.

Figure 5 shows the PID efficiencies for  $e^\pm$  (electron efficiency in the figure) and  $\pi^\pm$  obtained for the TPC and TRD at different momenta. It is seen qualitatively from Fig.5 — an enhancement of the pion efficiency with momentum increasing at fixed electron efficiency for both detectors. Figure 5,*f* demonstrates also a strong decrease of the pion efficiency for the TRD and TPC combination at momentum 6 GeV/*c*, taken as an example. It was found that this combined efficiency is very near to simple multiplication of those obtained separately for TRD and TPC.

The PID results are summarized in the Table where the pion rejection factor (the number reverse to the pion efficiency) is presented separately for the TPC, TRD and for a combination of these detectors. One can see from the Table that the pion rejection factor for the TPC and TRD combination (the last row) may be very large at  $p \leq 4$  GeV/*c* and strongly decreases at higher momentum. It should be noted that at  $p \simeq 1$  GeV/*c* proton contamination is most important because the proton rejection factor is only  $\sim 50$  at this momentum. This factor

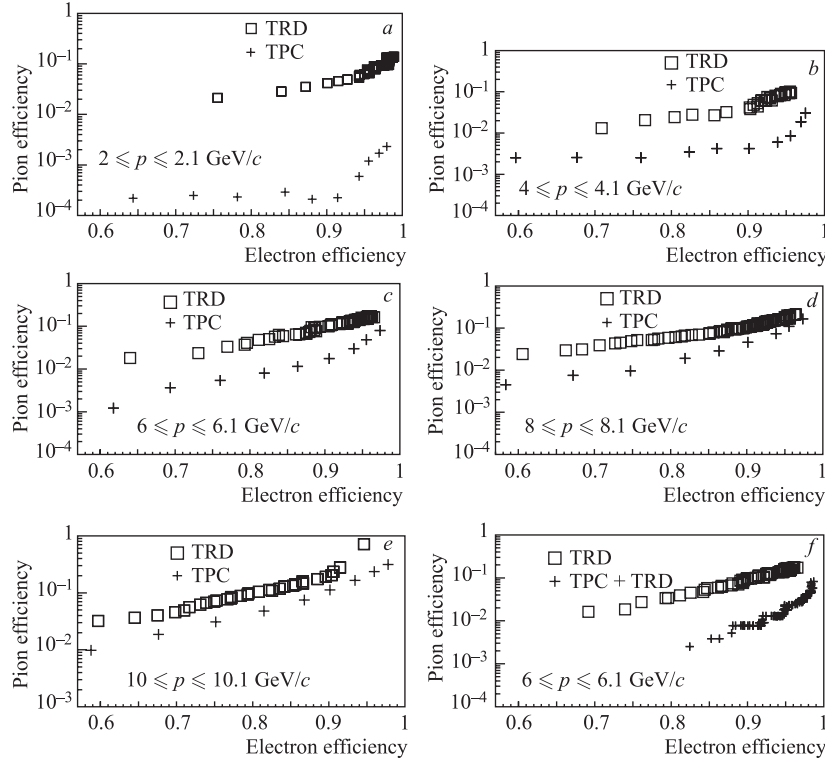


Fig. 5. Pion efficiency as a function of electron ( $e^\pm$ ) efficiency at different momenta for the TRD and TPC. The Fig. *f* shows the results for the TPC and the TPC + TRD combination at momentum 6 GeV/*c*

**Pion rejection in the TPC and TRD at electron efficiency 90% for different momenta**

$p$ , GeV/ $c$	1.5	2.0	4.0	6.0	8.0	10.0
Rejection in the TPC	2500	2000	400	50	25	12
Rejection in the TRD	40	30	25	10	8	5
Rejection in the TPC+TRD	$10^5$	$6 \cdot 10^4$	$10^4$	500	200	60

becomes comparable for protons and pions at  $p \simeq 1.5$  GeV/ $c$  and several times larger for protons as compared with the pion one already at  $p = 2$  GeV/ $c$ . We note also that more traditional but not the best algorithm has been used for the PID in the TRD. The Neural Network method, for example, is very promising since it allows one to increase the pion rejection factor to 2–3 (Subsec. 5.4.3 in [19], Sec. 3.3 in [34, 35]). However, the statistical errors are high enough ( $\sim 30\%$ ) for the pion rejection factors at  $p \leq 2$  GeV/ $c$  presented in the Table for both detectors and decrease to 10–15% at larger momenta. Besides, we assume more problems in the realistic experimental situation (for example, procedure of the corrections for the detector calibration and misalignment has not been taken into account). As a consequence, more pessimistic maximum pion rejection ( $\leq 10^4$ ) has been taken to obtain the  $\pi^\pm$  contamination at the next (second) step of the simulation.

**1.2. The Second (Fast) Step of the Simulation.** To carry out the fast simulation step all necessary sources of  $e^\pm$  were included to the AliGenCocktail generator (inside the AliRoot) creating the corresponding combination of the AliGenParam one. A charged particle density,  $dN_{\text{ch}}/dy = 2200$  at  $y = 0$ , has been supposed for the events according to the prediction in the ALICE PPR (Subsec. 1.3.1 in [18]). Mean numbers (from Poisson distributions) of the  $e^\pm$  sources per event were taken as following:

—  $170\pi^0$  and  $55\eta$  at  $p_t \geq 1$  GeV/ $c$  leading after decays to  $e^\pm$  at  $p_t \geq 1$  GeV/ $c$  — from the HIJING generator with charged particle density  $dN_{\text{ch}}/dy = 2200$  at  $y = 0$  (for impact parameter range 7–9 fm);

—  $0.018\rho^0$  and  $0.023\omega$  dielectron decays — from the HIJING generator taking into account the dielectron branching ratios;

—  $0.012 \phi \rightarrow e^+e^-$  decays — from RHIC experimental data  $\phi/\pi^- = 0.021$  [36, 37] and taking into account the dielectron branching ratio;

—  $0.02 J/\psi \rightarrow e^+e^-$  decays — from the TDR of TRD (see Sec. 12.2 in [32]);

—  $2.0(0.7)$  and  $0.1(0.04)$  semielectron decays of hadrons with charm and beauty, respectively, — have been calculated using the data presented in Table 7 of [38] and in Table 6.55 of [19] (Subsec. 6.6.3.5). The values in brackets take into account the factor ( $\sim 3$ ) of theoretical uncertainties for the charm and beauty total cross sections (see Table 3 in [38]);

—  $0.01\pi^\pm$  in the  $p_t$  range 1.0–2.5 GeV/ $c$  and  $0.05p/\bar{p}$  in the  $p_t$  range 0.5–1.5 GeV/ $c$  — from the PID study (see the previous section) and numbers of  $\pi^\pm$  and  $p/\bar{p}$  in different  $p_t$  intervals (this contamination is negligible at  $p_t \geq 2.5$  GeV/ $c$  for pions and at  $p_t \geq 1.5$  GeV/ $c$  for  $p/\bar{p}$ );

—  $0.4e^\pm$  — from gamma conversions using the impact parameter cut  $d \leq 0.1$  mm (see Fig. 2, *b* in the previous section).

Next,  $p_t$  and angles of  $e^\pm$  were smeared according to the shapes obtained at the first (detailed) step of the simulation considered in the previous section and then the new  $p_x$ ,  $p_y$ ,  $p_z$  components have been applied to calculate the effective mass of  $(e^+e^-)$  pairs. The particles only at  $p_t \geq 1$  GeV/ $c$  were selected for this analysis. Figure 6 shows the effective

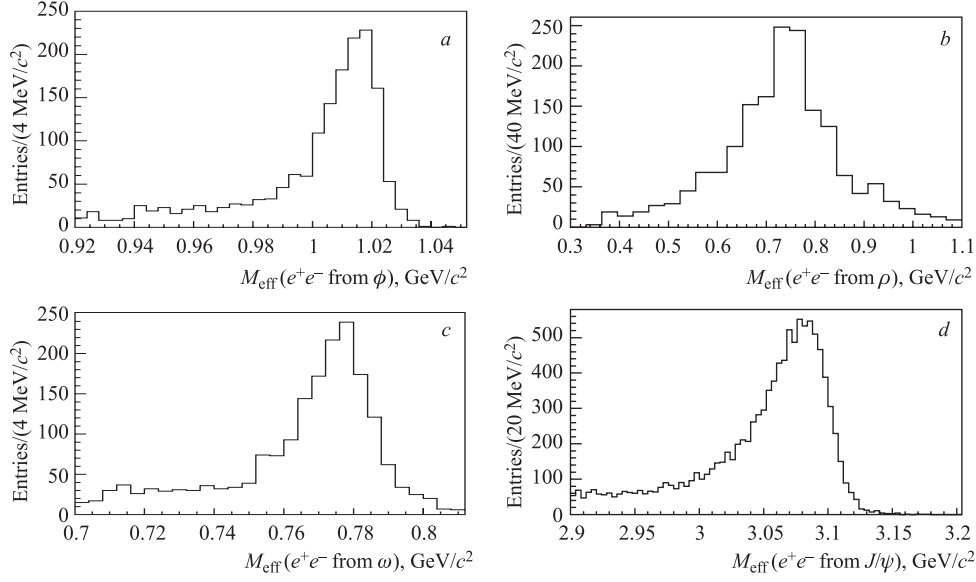


Fig. 6. Effective mass distributions of  $(e^+e^-)$  pairs from decays of  $\phi$  (a),  $\rho^0$  (b),  $\omega$  (c),  $J/\psi$  (d)

mass distribution of  $(e^+e^-)$  pairs taken from the different resonance decays. The asymmetric tails of the distributions are a consequence of the asymmetric  $p_t$  distribution shown in Fig. 2, a. This asymmetry is absent for  $\rho^0$  decays because of the large width of this resonance.

## 2. RESULTS

Figure 7 shows the spectrum of  $(e^+e^-)$  effective mass obtained from  $8 \cdot 10^6$  cocktail generator events. Difference between Fig. a and Fig. b is conditioned by the different con-

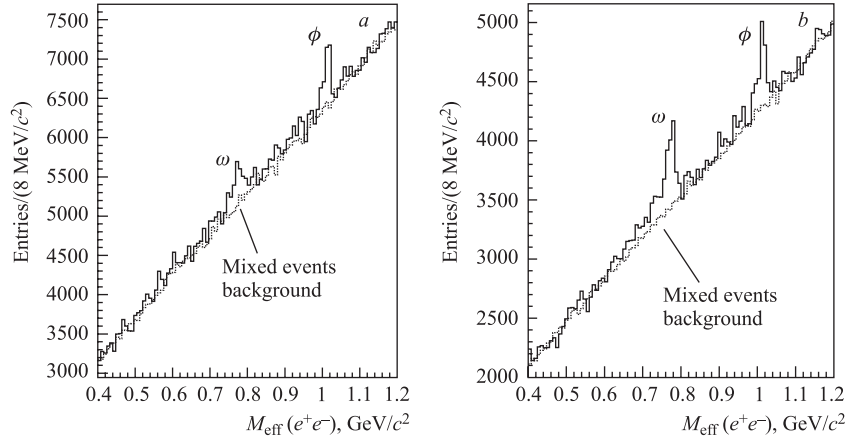


Fig. 7. Spectrum of  $(e^+e^-)$  effective mass for Pb-Pb events in the range of  $\rho$ ,  $\omega$  and  $\phi$  mesons. Mixed events background is also shown. The S/B values are  $\sim 0.1$  in plot a and  $\sim 0.15$  in plot b for both resonances. Difference between panels a and b is conditioned by the different contributions of hadrons with charm and beauty in the generator (see Subsec. 1.2)

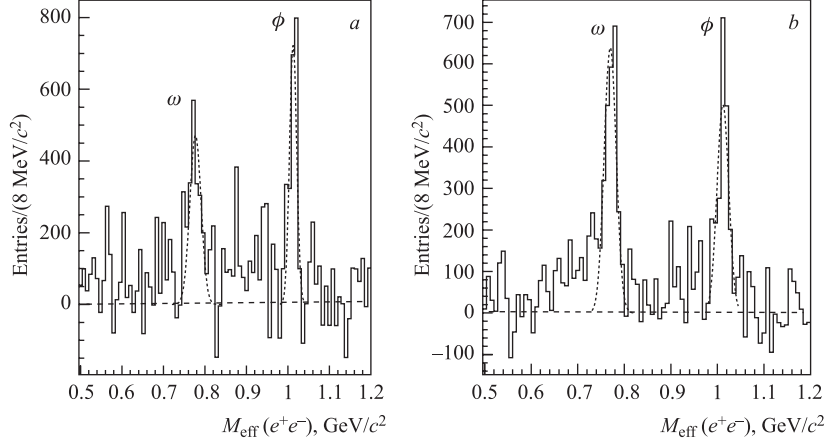


Fig. 8. Signals of  $\omega$  and  $\phi$  after background subtraction for Pb–Pb events. The curves are the fit results for the Gaussian function (see the text). The condition of difference between panels *a* and *b* is the same as in Fig. 7

tributions of hadrons with charm and beauty in the generator (see Subsec. 1.2) taking into account the theoretical uncertainties for the charm and beauty total cross sections (see Table 3 in [38]). The signals (S) of  $\omega$  and  $\phi$  are clearly seen over the combinatorial background (B) obtained by mixed events method. The S/B values are  $\sim 0.1$  in Fig. *a* and  $\sim 0.15$  in Fig. *b* for both resonances with statistical errors  $\sim 10\%$  (in the mass region  $\pm 12$  MeV/ $c^2$  around the maximum). The significance ( $S/\sqrt{S+B}$ ) numbers are  $\sim 12$  and  $\sim 15$ , respectively, in Figs. *a* and *b* recalculated for  $2 \cdot 10^7$  events, i.e., to statistics available within one month of ALICE operation ( $10^6$  s) with 40 central events taken per second (see Sec. 9.8 in [17] and Subsec. 3.18.4 in [18]) and also taking into account a running efficiency of 50%.

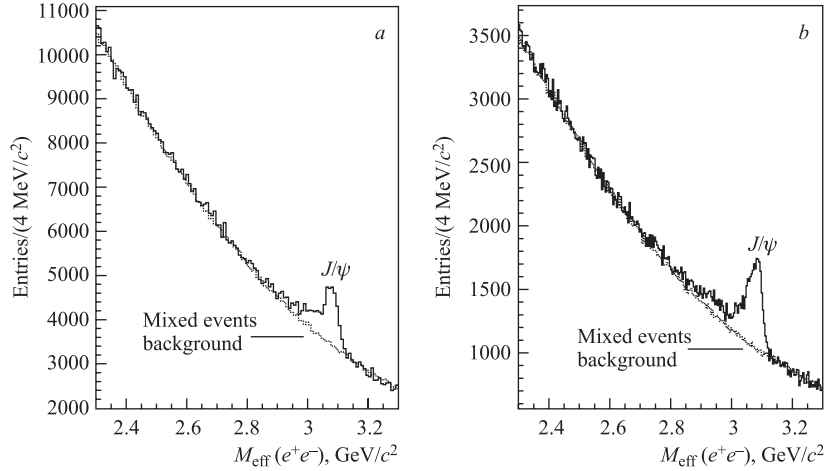


Fig. 9. Spectrum of  $(e^+e^-)$  effective mass for Pb–Pb events in the range of  $J/\psi$  resonance. Mixed events background is also shown. The S/B are  $\sim 0.4$  in plot *a* and  $\sim 0.6$  in plot *b*. The condition of difference between panels *a* and *b* is the same as in Fig. 7

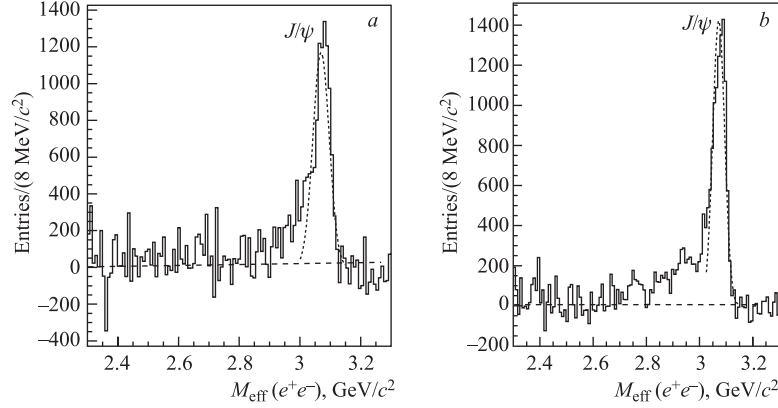


Fig. 10. Signals of  $J/\psi$  after background subtraction for Pb–Pb events. The curves are the fit results for the Gaussian function (see the text). The condition of difference between panels  $a$  and  $b$  is the same as in Fig. 7

The resonance signals after the background subtraction are shown in Fig. 8. The curves are the Gaussian fit results with the parameters:  $M(\omega) = (770.0 \pm 0.5) \text{ MeV}/c^2$ ,  $M(\phi) = (1012.0 \pm 0.5) \text{ MeV}/c^2$  and  $\sigma = 13.0 \text{ MeV}/c^2$  for both resonances and in the both Fig.  $a$  and Fig.  $b$ . It should be noted that  $\rho^0$  signal is not visible because of the large width.

The same results but in the effective mass range of  $J/\psi$  are demonstrated in Figs. 9 and 10. One can see the much better situation for  $J/\psi$  resonance as compared with the light vector mesons. The S/B are  $\sim 0.4$  in Fig.  $a$  and  $\sim 0.6$  in Fig.  $b$  with statistical errors  $\sim 3\%$  (in the mass region  $\pm 20 \text{ MeV}/c^2$  around the maximum). The significance values are  $\sim 40$  and  $\sim 50$  in plots  $a$  and  $b$ , respectively, for  $2 \cdot 10^7$  events. The results for the Gaussian fit are  $M(J/\psi) = (3072.4 \pm 0.4) \text{ MeV}/c^2$  and  $\sigma = 23.0 \text{ MeV}/c^2$ . It should be noted that this S/B result is near two times lower as compared with that presented in Subsubsec. 6.7.5.3 of [19] since  $e^\pm$  from gamma conversions have been taken into account in the presented simulation.

It is seen from the results that Gaussian fits lead to resonance masses visibly lower than those presented in the PDG. This difference is a consequence of the asymmetric shifts of the effective mass distributions shown in Fig. 6.

## CONCLUSIONS

Simulation study shows that  $\omega$  and  $\phi$  decays in  $e^+e^-$  pairs may be selected in ALICE detector for Pb–Pb collisions with values of S/B = 0.10–0.15 and significance number of 12–15 for statistics  $2 \cdot 10^7$  events. The same results but for  $J/\psi$  resonance are respectively 0.4–0.6 and 40–50. A mass shift by 0.7–1.5% as compared with experimental data (presented in the PDG) was found because the bremsstrahlung effect has not been taken into account during the tracking procedure.

It has been noted in Sec. 2 that the statistics  $2 \cdot 10^7$  events may be obtained within one month of ALICE operation.

REFERENCES

1. Johnson S. C. *et al.* // Phys. J. C. 2001. V. 18. P. 645.
2. Pal S. *et al.* // Nucl. Phys. A. 2002. V. 707. P. 525.
3. Rapp R. nucl-th/0701082v1. 2007.
4. Van Hees H., Rapp R. hep-ph/0711.3444v2. 2007.
5. Pisarski R. D., Wilczek F. // Phys. Rev. D. 1984. V. 29. P. 338;  
Shuryak E. V. // Nucl. Phys. A. 1991. V. 525. P. 3c.
6. Asakawa M., Ko C. M. // Phys. Lett. B. 1994. V. 322. P. 33; Phys. Rev. C. 1994. V. 50. P. 3064.
7. Agakishiev G. *et al.* // Phys. Rev. Lett. 1995. V. 75. P. 1272.
8. Angelis A. L. S. *et al.* // Eur. Phys. J. C. 2000. V. 13. P. 433.
9. Adamova D. *et al.* // Phys. Rev. Lett. 2003. V. 91. P. 042301.
10. Agakishiev G. *et al.* // Eur. Phys. J. C. 2005. V. 41. P. 475.
11. Araldi R. *et al.* // Phys. Rev. Lett. 2006. V. 96. P. 162302.
12. Afanasiev S. *et al.* nucl-ex/0706.3034v1. 2007.
13. Adamova D. *et al.* nucl-ex/0611022v3. 2008.
14. Koch P. *et al.* // Phys. Rep. 1986. V. 142. P. 167.
15. Rafelski J., Muller B. // Phys. Rev. Lett. 1982. V. 48. P. 1066;  
Bass S. A. *et al.* // Nucl. Phys. A. 1999. V. 661. P. 205.
16. Shor A. // Phys. Rev. Lett. 1985. V. 54. P. 1122;  
Koch P. *et al.* // Z. Phys. C. 1990. V. 47. P. 477.
17. ALICE Collab. Technical Proposal. CERN/LHCC 95-71, LHCC/P3. 1995.
18. ALICE Collab. Physics Performance Report. V. 1 // J. Phys. G: Nucl. Part. Phys. 2004. V. 30. P. 1517.
19. ALICE Collab. Physics Performance Report. V. 2 // J. Phys. G: Nucl. Part. Phys. 2006. V. 32. P. 1295.
20. Afanasiev S. V. *et al.* // Phys. Lett. B. 2000. V. 491. P. 59.
21. Xu Z. // Nucl. Phys. A. 2002. V. 698. P. 607c.
22. Adler C. *et al.* // Phys. Rev. C. 2002. V. 65. P. 041901.
23. Adler S. S. *et al.* // Phys. Rev. C. 2005. V. 72. P. 014903.
24. Friese V. // Nucl. Phys. A. 2002. V. 698. P. 487c.
25. Wills N. *et al.* // Nucl. Phys. A. 1999. V. 661. P. 543c;  
Alessandro B. *et al.* // Phys. Lett. B. 2003. V. 555. P. 147.

676 *Batyunya B., Vala M., Zaporozhets S. (for ALICE Collaboration)*

26. *Adamova D. et al.* // Phys. Rev. Lett. 2006. V. 96. P. 152301.
27. *Arnaldi R. et al.* // Eur. Phys. J. C. 2007. V. 49. P. 255.
28. *Batyunya B. et al.* // JINR Rapid Commun. 1997. No. 5[85]. P. 61; Internal Note/SIM ALICE/97-26. 1997;  
*Batyunya B. et al.* // Part. Nucl., Lett. 2005. V. 2, No. 2(125). P. 72;  
*De Caro A. et al.* Internal Note ALICE-INT-2003-067;  
*Akindinov A. et al.* // Eur. Phys. J. C. 2006. V. 45. P. 669–677.
29. *ALICE Collab.* Inner Tracking System. Technical Design Report. CERN/LHCC 99-12, ALICE TDR 4. 1999.
30. *ALICE Collab.* Time Projection Chamber. Technical Design Report. CERN/LHCC 2000-001, ALICE TDR 7. 2000.
31. *ALICE Collab.* Transition Radiation Detector. CERN/LHCC 99-13, LHCC/P3-Addendum 2. 1999.
32. *ALICE Collab.* Transition Radiation Detector. Technical Design Report. CERN/LHCC 2000-021, ALICE TDR 9. 2001.
33. *Sjöstrand T.* // Comp. Phys. Commun. 1994. V. 82. P. 74.
34. *ALICE Collab.* ALICE Technical Paper I. CERN. 2008.
35. *Wilk A.* Report in the ALICE Physics Week. Prague, 2008.
36. *Caines H.* // Nucl. Phys. A. 2002. V. 698. P. 112c.
37. *Antinori F.* Talk Presented at «QM2004», Oakland, Jan. 2004.
38. *Carrer N., Dainese A.* Internal Note ALICE-INT-2003-019v.3. 2003

Received on November 25, 2008.